



UNIVERSITY OF TRENTO
DEPARTMENT OF PHYSICS
BACHELOR'S DEGREE IN PHYSICS

~ . ~

ACADEMIC YEAR 2023–2024

FALSE VACUUM DECAY VIA BUBBLE FORMATION

Supervisor
Dr. Alessandro ZENESINI

Graduate Student
Giorgio MICAGLIO
227051

FINAL EXAMINATION DATE: January 18, 2025

To all my friends

Acknowledgments

I would like to thank all of my friends.

Abstract

This thesis analyses a BEC experiment and some data analysis

Contents

Introduction	1
1 Theoretical picture	3
2 Data analysis	5
2.1 Magnetization data	5
2.1.1 Bubble parameters and shot sorting	5
2.1.2 FFT analysis	6
2.1.3 Autocorrelation analysis	8
2.2 Density data	8
Conclusions	9
A Alberio	11
Bibliography	13
List of Figures	13
List of Tables	15

CONTENTS

Introduction

Chapter 1

Theoretical picture

The experimental platform is composed of a bosonic gas of ^{23}Na atoms, optically trapped and cooled below the condensation temperature. The initial spin state in which the system is prepared is $|F, m_F\rangle = |2, -2\rangle = |\uparrow\rangle$, with F being the total angular momentum of the atom ($\mathbf{F} = \mathbf{I} + \mathbf{J}$, takes into account the nuclear spin and the total angular momentum of the electrons) and m_F its projection on the quantization axis. The $|\uparrow\rangle$ state is then coupled to $|1, -1\rangle = |\downarrow\rangle$ through microwave radiation with amplitude Ω_R .

The trapping potential is harmonic in all three directions, but strongly asymmetric concerning the radial (ρ) and axial (x) directions. In fact, the trapping frequencies are respectively $\nu_\rho = 2$ kHz and $\nu_x = 20$ Hz, yielding an elongated system (cigar-shaped) with inhomogeneous density. The spatial size of the system is given by the Thomas-Fermi radii $R_\rho = 2$ μm and $R_x = 200$ μm . This particular setup is helpful for suppressing the radial spin dynamics of the condensate and thus being able to study its longitudinal properties.

In order to extract the density distribution, the two spin states are treated independently one from another, and two imaging sequences are obtained at the end of each experimental realization. Then, an integration along the transverse direction is performed, obtaining two 1D density profiles $n_\uparrow(x)$ and $n_\downarrow(x)$, from which one can extract the relative magnetization

$$Z(x) = \frac{n_\uparrow(x) - n_\downarrow(x)}{n_\uparrow(x) + n_\downarrow(x)}. \quad (1.1)$$

It is possible to study the two-component system by separating the treatment on the density ($n = n_\uparrow + n_\downarrow$) and the spin ($nZ = n_\uparrow - n_\downarrow$) degrees of freedom. While the density is described by a continuity equation, the spin behaviour is ruled by a magnetic mean-field Hamiltonian, that presents a first-order phase transition in the central region of the system when $\Omega_R < |k|n$, where $k \propto \Delta a$. At fixed values of Ω_R , the experiment can be tuned by the parameter δ , expressing the *detuning*. In general, the mean-field energy landscape $E(Z)$ is described by an asymmetric double-well, that becomes symmetric for $\delta = 0$. In the case of $\delta > 0$, the energy is minimized by positive values of Z , and the absolute minimum will correspond to

Chapter 2

Data analysis

Raw data is organized in a hierarchical system. At a fixed instant, the condensate's measured data are called a *shot* (it refers to the imaging process). Each shot is part of a series of them that can be analyzed as the time evolution of a single system: this series is called a *sequence*. Eventually, during a *day* of measurements, many sequences may be collected, and a selection of them will be studied in the following analysis. For each sequence, the experimental data contains also the radiation coupling Ω_R in a range between 200 and 800 Hz (it changes from one day of measurements to another) and the detuning δ .

A shot contains all the information on the system at a certain instant, including the two population densities, $n_{\uparrow}(x)$ for the atoms in the state $|\uparrow\rangle$ and $n_{\downarrow}(x)$ for the atoms in the state $|\downarrow\rangle$, distributed on a length scale from 0 to 400 pixels. The spatial resolution of the image is 1 pixel = 1 μm , so the two length units will be often used interchangeably. The magnetization data $Z(x)$ is calculated with Eq. (1.1) and, by definition, composed of a series of values ranging from -1 to 1 .

2.1 Magnetization data

Our focus here is to study the magnetization of the system, developing a method to analyze the effects of its bubble formation.

2.1.1 Bubble parameters and shot sorting

In order to study the bubble dynamics, the most interesting parameters to retrieve from a shot are the bubble center x_0 and width σ_B . However, not all shots contain a bubble, namely the ones taken when the bubble was not formed yet. We can easily classify the two types of shots by computing the magnetization average in the central region and using a threshold value of $Z_{\text{thr}} = -0.2$. The no-bubble shots will be useful later, when dealing with the noise frequency spectrum.

To find the bubble parameters, the magnetization data is fitted with a double-arctangent function

$$Z_{\text{fit}}(x) = -A \left[\frac{2}{\pi} \arctan\left(\frac{x - c_1}{w_1}\right) - \frac{2}{\pi} \arctan\left(\frac{x - c_2}{w_2}\right) \right] + \Delta, \quad (2.1)$$

where c_1 and c_2 are the centers of the arctangent "shoulders", and w_1 and w_2 are their characteristic widths. Then, for a better result, a further fit is performed on each shoulder with a

single-arctangent function

$$Z_{\text{fit}}(x) = -A \frac{2}{\pi} \arctan\left(\frac{x-c}{w}\right) + \Delta,$$

yielding the shoulder center c . Eventually, we obtain the bubble center $x_0 = (c_1 + c_2)/2$ and the bubble width $\sigma_B = c_2 - c_1$.

In some cases, especially when the bubble is narrow, the fitting procedure to optimize the parameters of Eq. (2.1)'s function fails and we are forced to use a gaussian profile such as

$$Z_{\text{fit}}(x) = -A \exp\left[-\frac{(x-c)^2}{2\sigma^2}\right] + \Delta,$$

with $x_0 = c$ being the bubble center and $\sigma_B = 2.335 \sigma$ its width.

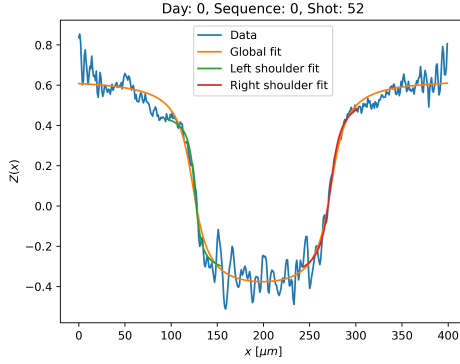


Figure 2.1: Example of double arctangent fit results performed on a shot.

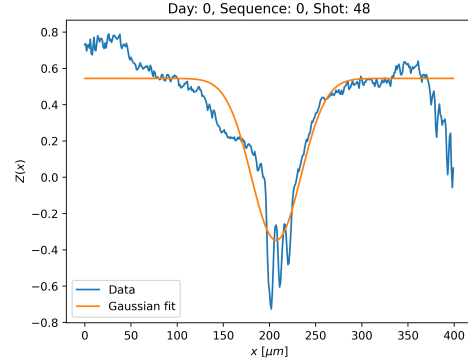


Figure 2.2: Example of gaussian fit results performed on a shot.

An example of fitting with the arctangent functions is provided in Fig. 2.1, while a gaussian fit is shown in Fig. 2.2.

Once the width is retrieved, it is useful to order the shots in a sequence by this parameter. This process lets us display the system evolution, in contrast to the original shot ordering based on the experimental time waited before observing the bubble. Furthermore, we can obtain a nicer picture by aligning the bubbles to their center. An example sequence is shown in Fig. 2.3 with a colormap displaying the magnetization profiles (blue is for positive Z and red for negative Z).

2.1.2 FFT analysis

Since we are interested in the dynamics of the bubble, energy propagation is an important feature to focus on. In order to study it, a spectral profile is much needed, from which one can extrapolate the main frequencies of the signal. We will first approach the problem of deriving such a profile using Fast Fourier Transform (FFT), an algorithm that implements the Discrete Fourier Transform (DFT) in an efficient manner. Given the input as a sequence of N discrete values Z_0, \dots, Z_{N-1} sampled with spacing Δx , by definition the DFT is a series of N discrete

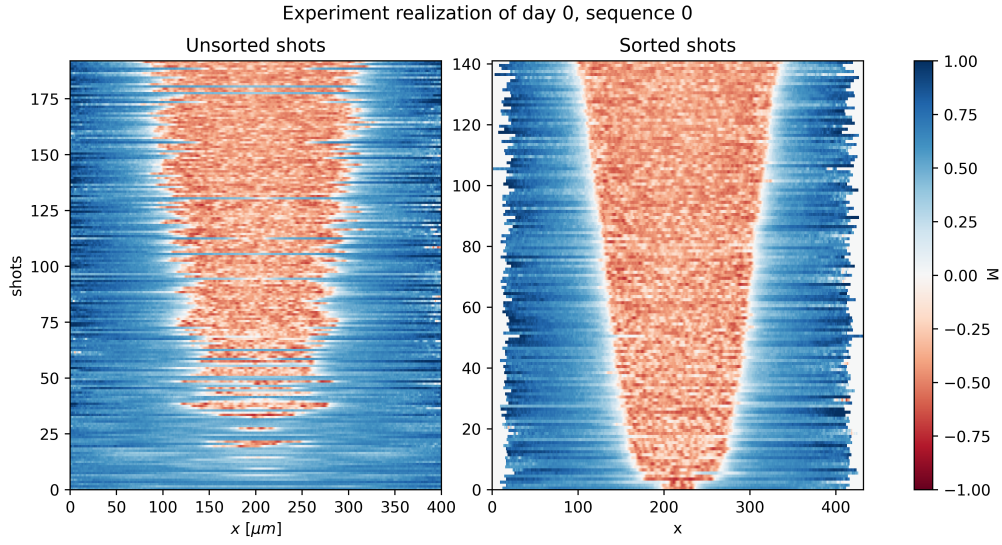


Figure 2.3: Shot sorting based on bubble width and alignment based on bubble center. Both parameters are estimated from the previous fitting procedure.

values $\mathcal{Z}_0, \dots, \mathcal{Z}_{N-1}$ spaced by $\Delta\nu = 1/(N\Delta x)$ such that

$$\mathcal{Z}_k = \sum_{n=0}^{n=N-1} Z_n e^{-2\pi i \frac{k}{N} n}.$$

When the input Z_n is real-valued, the transform is too, and it is also symmetric between positive and negative frequencies. The physical world contains only positive frequencies, so we will neglect the negative part of the transform.¹

¹This is achievable in Python using the function `rfft` instead of `fft`.

2.1.3 Autocorrelation analysis

2.2 Density data

Conclusions

CONCLUSIONS

Appendix A

Albero

List of Figures

2.1	Example of double arctangent fit results performed on a shot.	6
2.2	Example of gaussian fit results performed on a shot.	6
2.3	Shot sorting based on bubble width and alignment based on bubble center. Both parameters are estimated from the previous fitting procedure.	7

LIST OF FIGURES

List of Tables

